

Aerodynamic design and preliminary optimization of a commercial PrandtlPlane aircraft

Karim Abu Salem*, Vittorio Cipolla*, Marco Carini**, Michaël Méheut**, Stylianos Kanellopoulos**, Vincenzo Binante*** and Marco Maganzi*°

* University of Pisa, Department of Civil and Industrial Engineering, Aerospace Section
Via G. Caruso 8, 56122, Pisa (PI), Italy
karim.abusalem@gmail.com

** ONERA - The French Aerospace Lab, Meudon, France

*** SkyBox Engineering S.r.l., Pisa, Italy

*° Cubit S.c.a.r.l., Via Giuntini 13, 56021 Cascina, Italy

Abstract

The paper aims to present the phases and the achievements of the aerodynamic design activities carried out on a box-wing aircraft, called PrandtlPlane, proposed as a sustainable solution for the fulfilment of the more and more demanding requirements of the fast-growing air transport. The activities here presented are included in the on-going Project PARSIFAL (“Prandtlplane ARchitecture for the Sustainable Improvement of Future AirPLanes”), funded by European Union under the Horizon2020 Program. Starting from the conceptual aerodynamic design of the PrandtlPlane architecture, the paper follows the development of the aerodynamic design, dealing with the preliminary definition of a reference configuration, which performances have been evaluated with both low and high fidelity tools, and the optimization procedure for the improvement of cruise performance.

1 Introduction



Figure 1: Concepts for Blended Wing Body from “Silent Aircraft Initiative”, Truss Braced Wings from “SUGAR” project and Box-Wing from “PARSIFAL” project

The study of concepts for disruptive aircraft configurations, such as the ones shown in Figure 1, is a possible way to face the challenges the air transport sector will have to face in the next decades. Such challenges concern the fast-growing demand of air transport, today limited by both environmental and logistic constraints. Although the relevant scenario for this challenge has a worldwide size, the studies carried out in Europe in the last years ([1], [2], [3]), have led to the definition of a set of specific objectives:

- satisfy the increase of air traffic demand, which is expected to double about 20 years;
- reduce CO₂ and NO_x emissions and noise per passenger-kilometres;
- reduce to 4 hours the time required to complete a door-to-door journey within Europe.

Among the proposed disruptive aircraft configurations, the Box-Wing has been studied since early 1990s at University of Pisa, where the attention has been focused on the possible applications in aviation of the so-called *Best Wing System* (BWS) concept, due to L. Prandtl. In [4], he demonstrated with an approximated approach that, for given wingspan and lift, the multi-wing system with minimum induced drag is a box-wing a proper normal force distribution. The following studies in Pisa ([5]) have shown that a closed-form-solution of the optimal lift distribution exists and that it is possible to apply the BWS concept to aircraft design, taking constraints from other disciplines, such as flight mechanics, structures and propulsion integration, into account. In Prandtl’s honour, the aircraft architecture based on the BWS has been then called “PrandtlPlane” (PrP).

Such research activities have demonstrated that beside the main advantage of reducing the induced drag, the PrP, configuration can bring further benefits, such as:

- smooth stall behaviour and post-stall characterized by only a partial reduction of manoeuvrability and controllability ([6]);
- pitch control achievable by using counter-rotating elevators (on both front and rear wings) which can introduce a pitching moment without perturbation to lift ([7]);

- higher pitch damping than in the case of a wing-tail configuration, with benefits in terms of comfort and safety ([8]).
- applicability to aircraft of different size and category ([9], [10], [11]) with different fuels, including hydrogen ([12]).

Concerning the above mentioned future challenges of air transport, the PrP is a potential solution since the one way to exploit the aerodynamic advantages of the BWS is to improve the payload capabilities of a conventional airplane, while keeping the same wingspan. In other words, for a given wingspan, it is possible to have a larger fuselage, without penalties in span efficiency, since this is improved by adopting the BWS. As confirmed also by other research (e.g. [13]), this way the improved L/D ratio of the PrP layout, can turn into an improvement of the payload without penalizations in terms of fuel consumption, while keeping the same overall aircraft dimensions.

Given such context, in 2017 the European Union, through the Horizon 2020 programme, has funded a research project called PARSIFAL (“Prandtlplane ARchitecture for the Sustainable Improvement of Future AirPLanes”), coordinated by the University of Pisa with Delft University of Technology (Netherlands), ONERA (France), ENSAM (France), DLR (Germany) and SkyBox Engineering (Italy) as partners.

The present paper aims at presenting the aerodynamic design activities carried out within PARSIFAL, focusing on the several phases which have led from the conceptual design to a optimization-driven refinement of the candidate configuration.

2 Conceptual aerodynamic design

In the PARSIFAL project, the definition of the aircraft design specification has been carried out by taking market analysis into account; in particular, the expected air traffic demand from 2032 has been analysed, as described in [15]. This time horizon has been chosen in accordance with the supposed time to market of an innovative configuration such as the PrandtlPlane. The graph in Figure 2 shows the forecast of a significant increase in passenger traffic demand, especially in the short-to-medium-range segment.

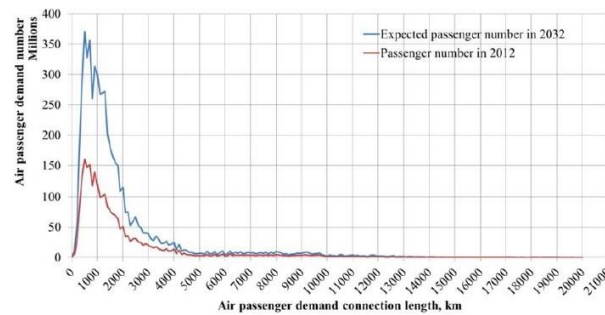


Figure 2: Air passenger demand for 2032 [15]

The outputs of the market analysis, together with the analysis of the current operational scenario of commercial aircraft, has allowed for the definition of Top Level Aircraft Requirements (TLARs) [16][17]. These specifications represent the main drivers of the design process and influence the most important design choices, starting from the macroscopic ones carried out during the conceptual design phase. The most relevant TLARs for the initial design decisions are the number of passengers and the nominal range. The PrandtlPlane developed within the PARSIFAL project aims to satisfy in a sustainable way the wide increase in continental traffic expected in the coming decades; therefore, the operating scenario of the PrP is the one of continental routes with a larger number of passengers with respect to the competitors that currently operate in this sector. The design field for an aircraft of this type is shown in the diagram in Figure 3; currently, there are not conventional aircraft capable of operating in this market segment.

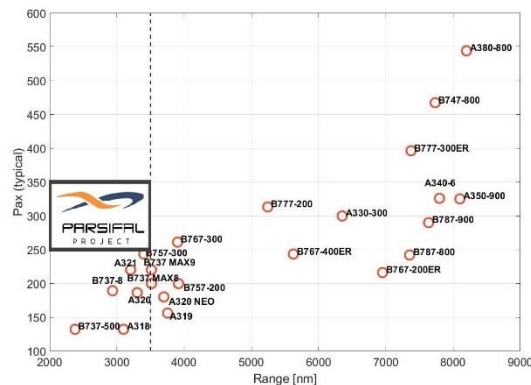


Figure 3: PARSIFAL market positioning (passengers-range)

A further constraint that significantly influences the aerodynamic design of the aircraft is the one related to the maximum wingspan; for the PrP developed in PARSIFAL, the maximum wingspan is set equal to 36 meters, as for the single-aisle aircraft currently operating in the short-to-medium range (Airbus A320 and Boeing 737 families). The limits on the maximum wingspan are defined by international standards [18]; in the case of PARSIFAL, it has been decided to maintain the same global dimensions of competitor aircraft in order to face the problem of airport saturation [19]. However, the aircraft aims to carry a larger payload thanks to the aerodynamic advantage of a lifting system designed according to the Best Wing System (BWS) theory. In order to embark a larger number of passengers than single-aisle aircraft and to maintain the same maximum dimensions, it has been necessary to consider configurations with fuselage sections capable of housing an appropriate number of seats. It is not possible to accommodate the required number of passengers in a single-aisle fuselage so two different alternative solutions have been identified, as shown in Figure 3; a solution with a double aisle and a single passenger deck ('SD', left in Figure 4) and a solution with a single aisle and a double passenger deck ('DD', right in Figure 4). Both solutions can hold standard LD3-45 containers.

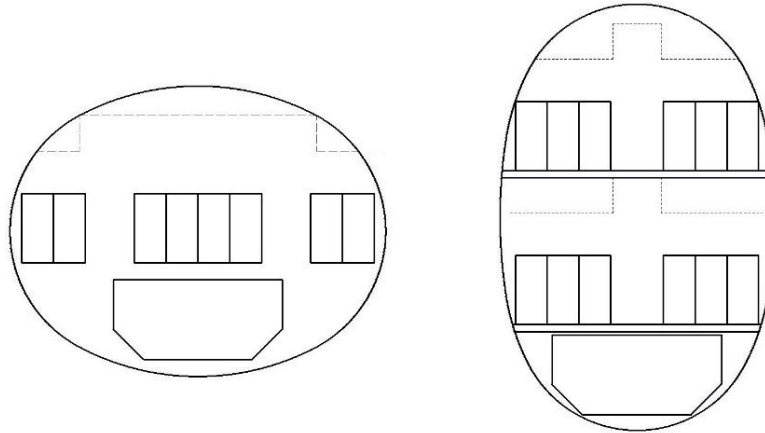


Figure 4: Cabin layouts studied in PARSIFAL: double aisle / single deck (left) and single aisle / double deck (right)

In addition, three different fuselage lengths have been considered for each cabin section in order to cover a wide range of possible payloads. The lengths considered are 36, 39 and 42 meters. In this conceptual design phase low-fidelity models, but very fast, have been used to estimate the weights and performance of the different configurations [20]; with these input data it has been possible to initialize the aerodynamic design. Table 1 summarizes the main characteristics of the families of aircraft analysed; the design weight (W_{des}) is set equal to the weight estimated at 25% of the cruise length :

Table 1: Aircraft families characteristics

Family	Single Deck (SD)			Double Deck (DD)		
	36	39	42	36	39	42
Fuselage Length [m]	36	39	42	36	39	42
Max Number of Passengers	248	280	304	270	318	366
W_{des} [tons]	105.5	117.3	126.1	113.6	131.1	148.4

The reference flight condition has been selected on the basis of data relating to aircraft operating in the same scenario selected in PARSIFAL; in particular, the cruise altitude has been set equal to 11000 meters and the cruise Mach equal to 0,79. The sketches in Figure 5 show two generic solutions for the 'SD' and 'DD' configurations.

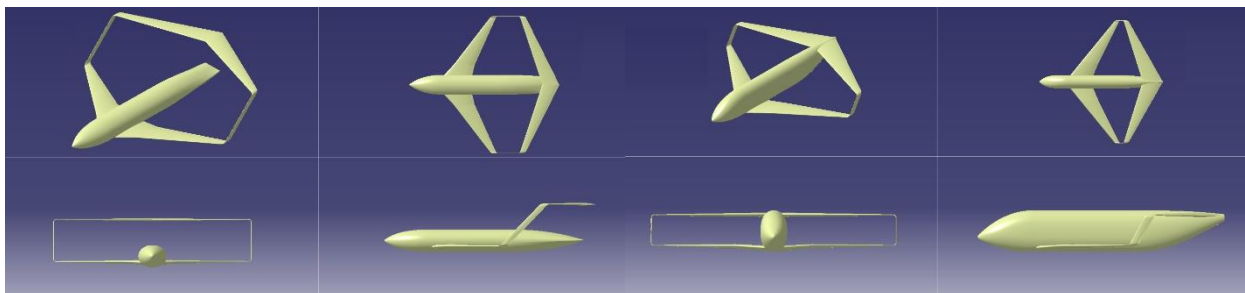


Figure 5: 3D sketch of two generic PrandtlPlane configurations ('SD' left, 'DD' right)

The initial aerodynamic design for the considered configurations has been carried out using an in-house tool called AEROSTATE (*AERodynamic Optimization with STATic stability and Trim Evaluator*) [21]; this tool uses a low fidelity aerodynamic code, based on the Vortex Lattice Method (VLM) [22]. These solvers are very useful in the

early stages of the design since they provide information on a very large number of configurations with low computational time. Since the aircraft performances have to be evaluated in transonic regime, it has been necessary to introduce some tuning to the aerodynamic evaluation procedure, as described in [23]. Moreover, given the significant differences between the compared fuselages, the effect on the drag of the fuselage is taken into account using the component drag model proposed in [20]; other features of the AEROSTATE code are described in [24] and [25]. The information on aerodynamic performance can therefore be used to perform macroscopic comparisons between different configurations and to detect correlations between the main performances and design parameters. The tool uses an aerodynamic optimization procedure to identify several configurations; this procedure is defined as follows:

$$\begin{cases} \min(-f(\mathbf{x})) \\ g(\mathbf{x}) \geq 0 \\ h(\mathbf{x}) = 0 \\ lb < \mathbf{x} < ub \end{cases} \quad (1)$$

where x is the vector of the design variables, $f(x)$ is the objective function (fixed equal to the aerodynamic efficiency, L/D), $g(x)$ and $h(x)$ are the sets of inequality and equality constraints, and lb and ub represent the lower and upper boundaries of the variation of the design variables, thus defining the design space. In these preliminary analyses, the design variables selected for each lifting surface are: chords and twists for a number of reference sections (root, kink and tip) and sweep and dihedral angles for the corresponding wing-bay; the relative longitudinal position of the two lifting surfaces is also a design parameter. The main constraints are related to the feasibility of the configurations evaluated, and concern aspects inherent to flight mechanics, aerodynamics and geometry. The set of the most relevant constraints is shown below:

$$W_{des} - \varepsilon_L \leq L(\mathbf{x}) \leq W_{des} + \varepsilon_L \quad (2)$$

$$\varepsilon_M \leq M(\mathbf{x}) \leq \varepsilon_M \quad (3)$$

$$SM_{\min} \leq SM(\mathbf{x}) \leq SM_{\max} \quad (4)$$

$$(W/S)_{\min} \leq (W/S(\mathbf{x}))_{\text{wing}} \leq (W/S)_{\max} \quad (5)$$

$$\max(c_l(y)) \leq c_{l\max} \quad (6)$$

$$\lambda_{\text{bay}} < 1 \quad (7)$$

where equations (2) and (3) represent vertical and pitch equilibrium constraints (L is the lift, W_{des} is the design weight, M is the pitching moment, ε is a tolerance defined by the designer), equation (4) is the constraint on longitudinal static stability (SM is the Static Margin of stability), (5) fixes the constraints on the wing loading (W/S) of each lifting surface, (6) imposes the maximum limits on the local lift coefficient ($c_l(y)$) in any spanwise section, and (7) represents the constraint on the taper ratio (λ) of each bay. The wingspan is fixed at 36 meters. In addition to these most relevant constraints, the designer may introduce other constraints depending on the particular problem addressed.

The optimization procedure in AEROSTATE searches for the minimum through a strategy that combines local and global algorithms, as described in detail in [21]. In this way, for each optimization run, a group of configurations with different characteristics is obtained as output; each configuration represents a local minimum (compatible with constraints) found during the progress of the calculation. This strategy is very useful at this early stage of the project, since it allows to evaluate the performance of a large number of configurations and to identify performance trends among different groups of solutions, as described below.

AEROSTATE has been used to evaluate several configurations for the 'SD' and 'DD' families (of which two examples are shown in Figure 6); in particular, configurations with different limits on maximum wing loading have been evaluated (400, 500, 600, 700 kg/m², referring to the front wing), and comparisons have been made for different configurations having fuselage length equal to 36, 39 and 42 meters.

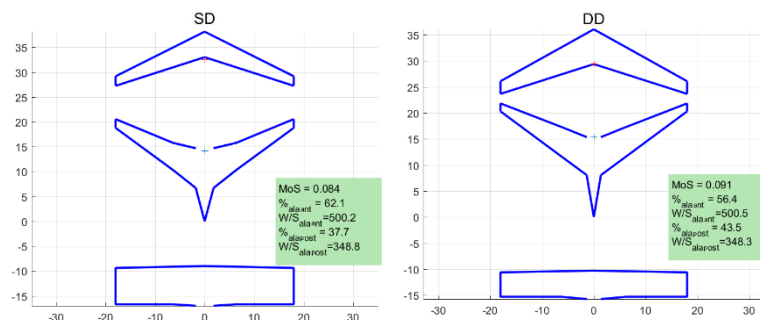


Figure 6: Two generic outputs of AEROSTATE ('SD' left, 'DD' right)

Although the aerodynamic solvers used in this phase are classified as low fidelity tools, some relevant information for the development of the aerodynamic design can be extracted. The graphs in Figure 7 show the improvement of aerodynamic efficiency (in terms of percentage increases with respect to the worst configuration) versus the variation of the wing loading, for the families 'SD' and 'DD', and for each fuselage considered. Each marker in the graph relates to a generic configuration (e.g. Figure 6), which is a local minimum of the optimization procedure; it is possible to identify the different groups of configurations obtained by increasing the limit on the maximum wing load constraint (according to the values previously indicated). From these graphs it is possible to deduce that:

- the aerodynamic efficiency of the 'SD' family is better than the 'DD' family in each case;
- the aerodynamic efficiency of the configurations improves as the wing loading increases.

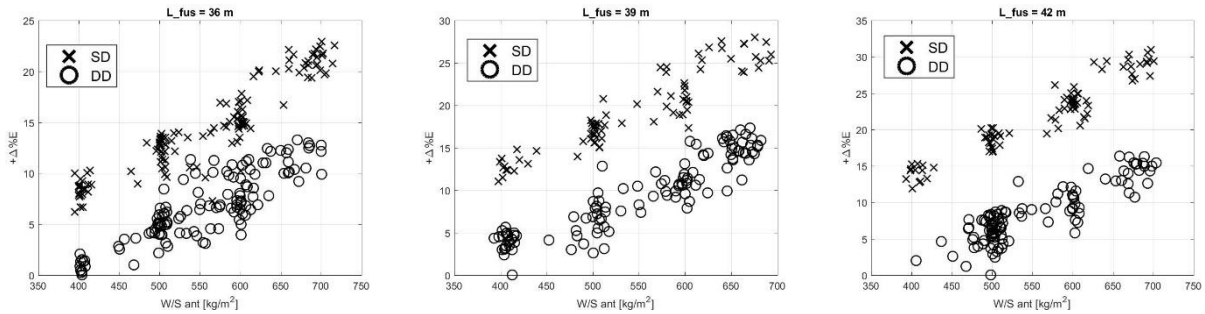


Figure 7: Aerodynamic efficiency versus front wing loading

The better performance of the SD family compared to the DD family is due to a lower fuselage drag and to a lower wetted surface of the lifting surfaces. The 'DD' configurations, in fact, for each fuselage length considered, have to equilibrate a larger weight and, therefore, given the same lift coefficient, they must necessarily have a larger reference surface, as can be seen from the graphs in Figure 8. Moreover, since the maximum wingspan is constrained, the lifting surfaces of the 'DD' configurations have a lower aspect ratio than the 'SD' configurations, also penalizing the contribution to induced drag.

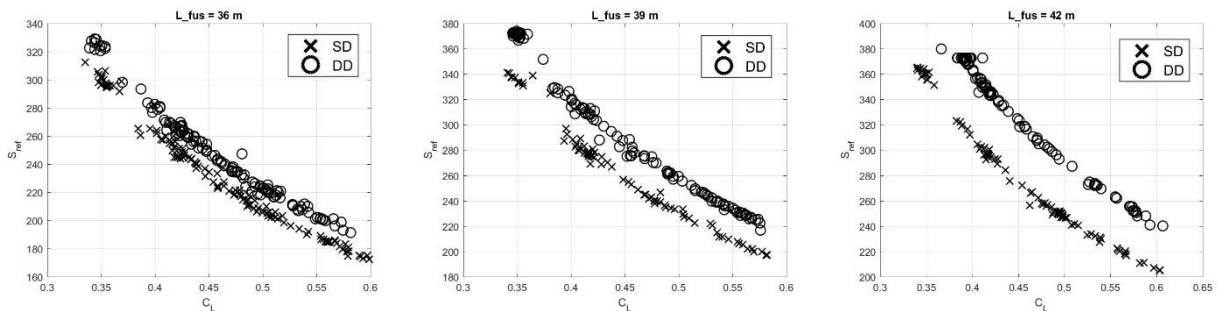


Figure 8: Reference surface variation with lift coefficient

The trends identified varying the wing loading are in accordance with the theories of the Best Wing System: the increase in induced drag resulting from the increase of C_L is lower than the typical trends of conventional aircraft, thanks to the higher span efficiency [5]; this results in a significant advantage in terms of aerodynamic efficiency, as can be seen in Figure 9. However, it is important to underline that phenomena associated to drag rise are not detectable by this model.

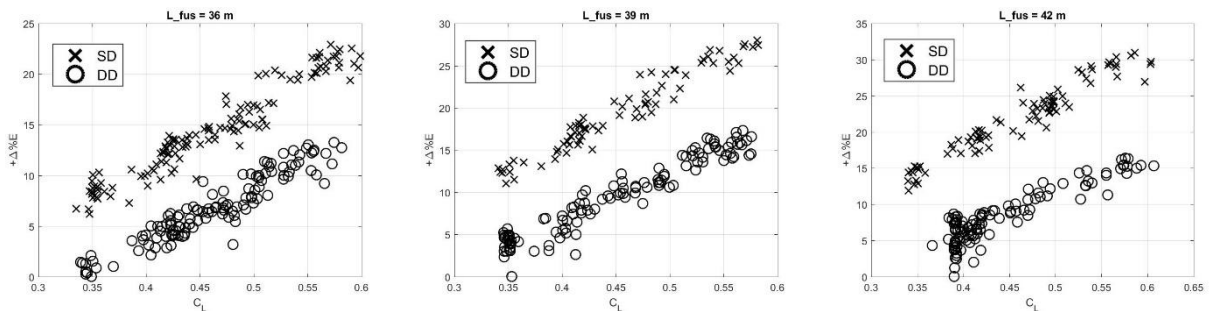


Figure 9: Aerodynamic efficiency versus lift coefficient

In the graphs of Figure 10, the results relative to the numerous configurations proposed in the previous graphs are represented as average values of the aerodynamic efficiency of each group of configurations. In a direct comparison,

the performance advantage of the 'SD' configuration compared to the 'DD' is evident. This is true even considering that the 'DD' is capable of carrying a larger payload than the 'SD' (for the same fuselage length): for example, the 'SD' configuration with a 42 meter fuselage (304 passengers) has a higher average aerodynamic efficiency than the 'DD' configuration with a 36 meter fuselage length (270 passengers). The gap becomes clear if we consider the 'SD' configuration with a 39 meter long fuselage, which has a comparable number of passengers (280). The 'SD' configuration with a 36 meter fuselage, while having the best overall performance, underperforms from the point of view of the maximum number of passengers (248); this limit, in fact, is too close to that of existing conventional aircraft (i.e. Airbus A321) and therefore may not justify the introduction of a disruptive configuration.

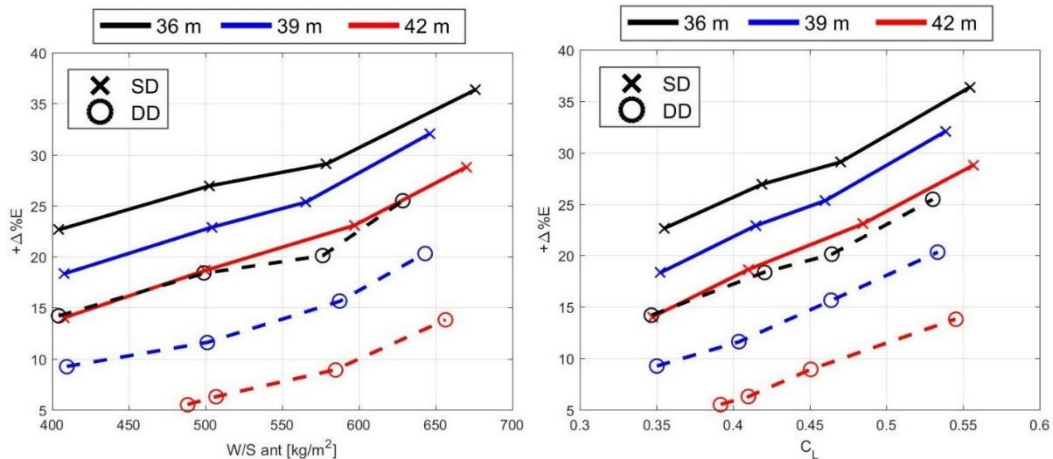


Figure 10: Average results for PrandtlPlane families: aerodynamic efficiency versus front wing loading and C_L

There are additional aerodynamic disadvantages for the 'DD' configuration:

- the rear wing must be mounted at the end of the fuselage, as shown in Figure 4; this is necessary because the height of the fuselage is very large, and installing the rear wing on top of the fins (as is possible for the 'SD' configuration [17]) would be unfeasible. This limitation causes a lower height/span ratio of the box-wing, and consequently a higher induced drag [5];
- installing the upper wing in the rear part of the fuselage makes critical the design of the wing-fuselage connection, especially for the aerodynamic performance in transonic; as evidenced by the results of high-fidelity CFD analysis on a test-case configuration, intense shock waves arise in the connection zone that cause large areas of separation of the boundary layer. It is necessary to provide a properly optimized connection in this region, in which the fuselage shape is constrained by other requirements;

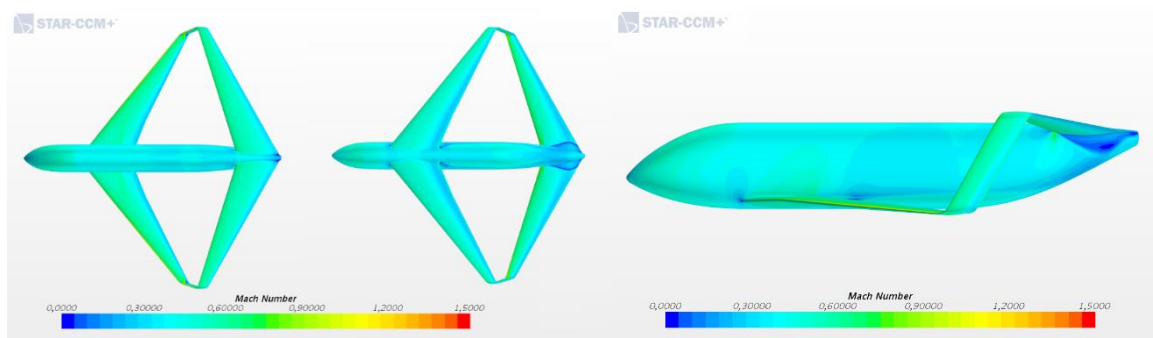


Figure 11: Mach contours on a test-case 'DD' configuration

- The 'DD' configurations are heavier than the respective 'SD' configurations (for the same fuselage length) and could fit into the wake-turbulence ICAO category beyond M, which instead is the reference target.

Following the considerations made so far, the choice has been to develop the 'SD' configuration with a fuselage length of 42 meters in the following phases of the aircraft design.

3 Preliminary aerodynamic design

After selecting the type of configuration to be developed, the second phase of the aerodynamic design has been started. The configurations analysed and developed in this phase are obtained through the same optimization procedure described in the previous section, but with refined boundaries and constraints; this tuning has been made following the results obtained from a CFD analysis campaign [26]. Some transonic performance information have been obtained focusing both on macro-parameters and local issues. For example, the aerodynamic efficiency for configurations with similar geometric characteristics but with different design wing loading has been investigated (Figure 12). It has been detected that, in transonic cruise, increasing the wing loading causes a decrease in aerodynamic efficiency, due to the arise of shock waves.

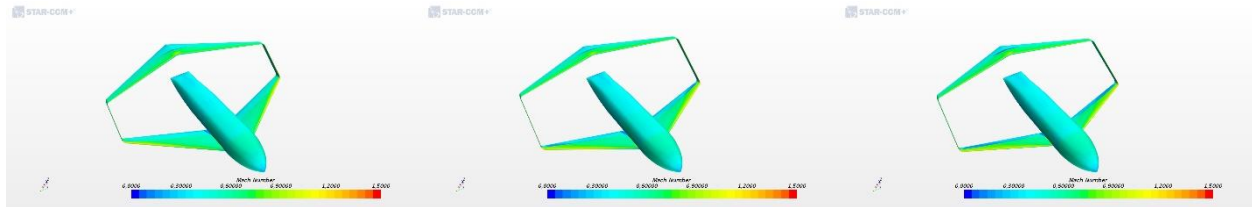


Figure 12: Mach contours on configurations with different wing loading

From these analyses it has been possible to understand that a conservative approach is useful in this phase of the aerodynamic design; this is mainly related to the need for using low fidelity aerodynamic tools, that cannot predict transonic phenomena reliably. For example, it is convenient to limit the design lift coefficient, and so the design wing loading, in order to be far from detrimental drag rise effect; this is in opposition to the subsonic performance of the BWS, that has its best aerodynamic behaviour at high C_L .

Weight estimation has been improved by using approximate models of higher fidelity [27]. The weight verification has been then carried out (for the configurations developed in the following phases of project) with even more accurate models, as described in [28]. For the configuration developed in this phase a MTOW of 120 tons has been estimated.

The graphs in Figure 13 show the aerodynamic efficiency trends with the variation of the design wing loading; as in the cases analysed in the previous paragraph, there is an increase in aerodynamic efficiency as the load increases. However, it has been necessary to find a trade-off between the performance of the BWS in incompressible flow (better performance at high wing loading) and those in transonic, where it is necessary to avoid high values of wave drag.

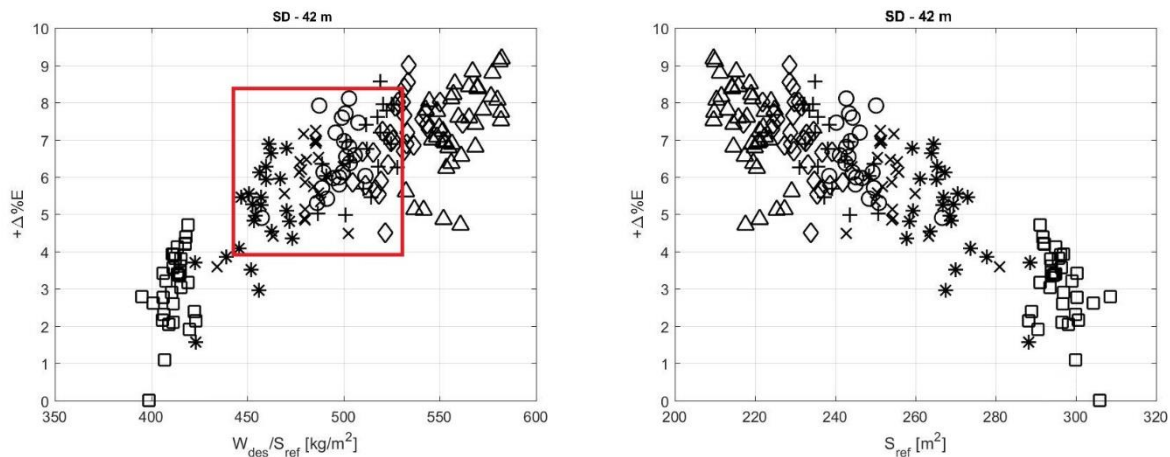


Figure 13: Aerodynamic efficiency versus front wing loading

For this reason, the initial reference configuration has been searched in a field that could guarantee the trade-off between the two different requirements on wing loading (qualitatively represented by the red square region in Figure 13). The configuration chosen in this phase, in fact, will be subject to high fidelity refinement (see Section 4), therefore a conservative and improvable configuration has been selected, with good performances (but not near to the optimum achievable) but far from macro critical issues. The preliminary evaluation of the aerodynamic performance of the selected configuration has been confirmed by high-fidelity CFD analyses (Figure 14).

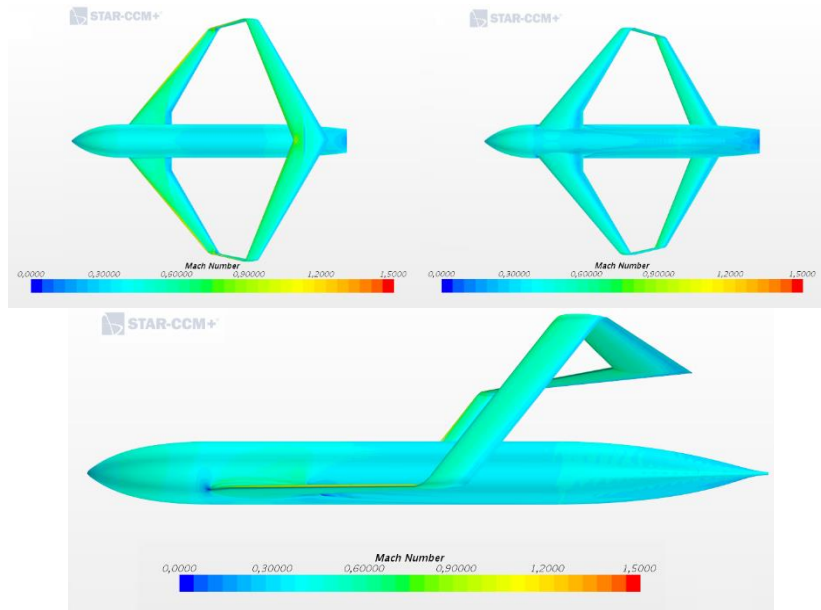


Figure 14: Mach contours the baseline PrandtlPlane configuration

4 Hi-Fi CFD analyses and improved boxwing design

In this section, results obtained from CFD analyses and optimization studies carried out at ONERA on the isolated boxwing lifting-system are presented. High-fidelity RANS computations have been performed to assess the aerodynamic performance of the baseline boxwing configuration while an Euler-based workflow is employed for its preliminary optimization by addressing the twist distribution. In both cases, CFD computations are supplemented by a detailed far-field drag post-processing to investigate the impact of the different drag sources (induced, wave, pressure and viscous dissipation) on the aerodynamic performance.

4.1 Baseline aerodynamic performance: far-field drag analysis

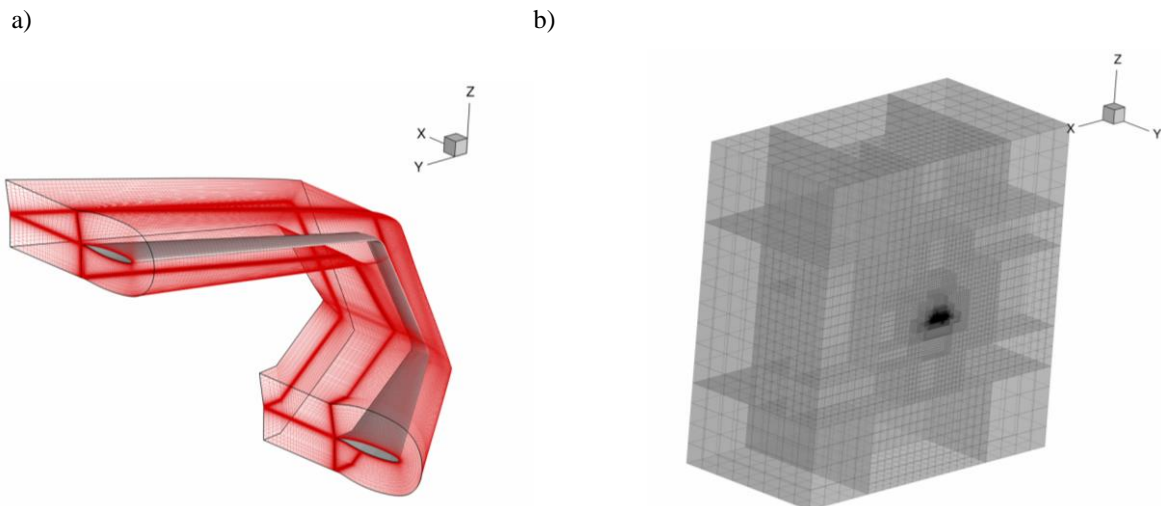


Figure 15: Chimera mesh components. (a) Boxwing mesh with $\sim 15.3 \times 10^6$ cells. (b) Background Cartesian octree mesh with $\sim 1.1 \times 10^6$ cells.

RANS computations have been performed using the in-house ONERA cell-centred finite-volume solver elsA (ONERA-Airbus-Safran property). In particular, a Chimera approach is employed to handle the considered geometry, with a body-fitted structured grid around the boxwing and a Cartesian-octree background grid, automatically created using the *Cassiopée* software library [29]. The normal wall spacing is kept almost uniform

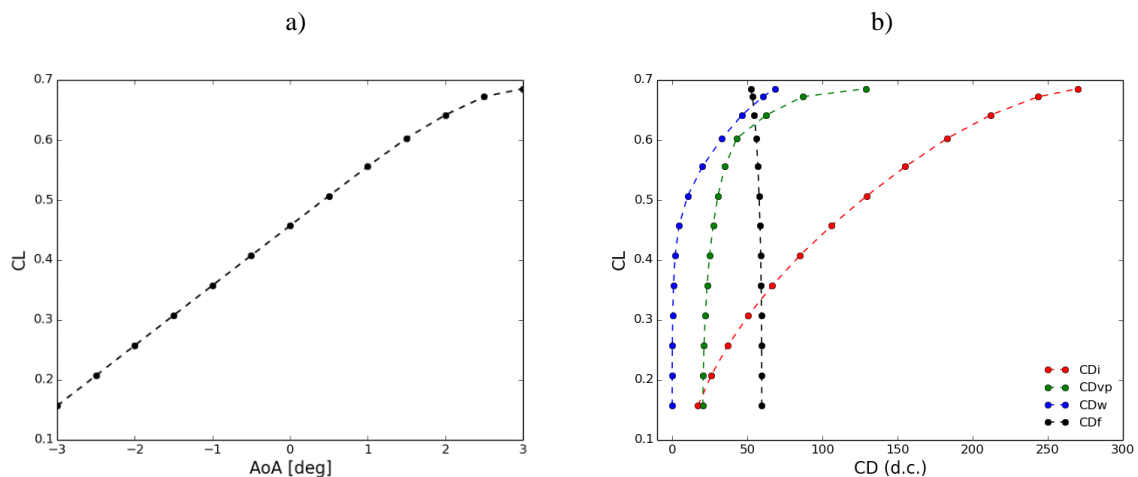
everywhere with a size of $\sim 5 \mu\text{m}$, corresponding to a maximum $y^+ \sim 0.8$ for the considered cruise conditions of $M=0.79$ and altitude of 11.0 km. The background domain features extends for ~ 400 m away from the boxwing surface along the xyz directions. These grids are shown in Figure 15. Once the different grids are assembled, the total number of cells for the half-boxwing model is of $\sim 16.0 \times 10^6$. No-slip boundary conditions are applied on the wall surface while on the boundary of the Cartesian background grid, symmetry conditions applies on the plane $y=0$ and far-field conditions are imposed on the remaining boundaries. The RANS equations with the QCR version of the Spalart-Allmaras turbulence model [30][31] and the Jameson scheme [32] for the inviscid flux discretization are converged towards a steady solution by using a backward-Euler pseudo time stepping technique with a LUSSOR implicit stage and a multigrid acceleration. The aerodynamic coefficients have been then calculated from the obtained converged CFD solutions using the far-field drag extraction post-processor *ffd* developed at ONERA. Indeed this software enables a refined drag through an accurate breakdown into lift-induced, viscous (sum of friction and viscous pressure) and wave components. More precisely an exact near-field far-field balance reads:

$$CD_p + CD_f = CD_{vp} + CD_w + CD_i + CD_f,$$

where the left-hand side corresponds to the *near-field decomposition* in terms of pressure and friction drag contributions, CD_p and CD_f , respectively, while the right-hand side provides the far-field drag phenomenological breakdown CD_{vp} being the viscous pressure drag, CD_w the wave drag and CD_i the induced drag coefficients. The far-field drag formulation implemented in *ffd* is derived from that introduced by Van der Vooren and Destarac in [33]. Further details of the ONERA's so-called one vector variant can be found in [34].

The lift and the far field drag polar curves are illustrated in Figure 16(a) and Figure 16(b), respectively. The stall onset occurs quite early, at an incidence of $\sim 3.0^\circ$, which limits the maximum lift coefficient around $\sim 0.65-0.7$. As expected, the contribution of the viscous dissipation is almost insensitive to the load condition. The wave drag is very small at negative angles of attack and gradually increases up to ~ 50 d.c. for $CL > 0.6$. A sudden drag rise occurs for the viscous pressure drag when CL increases over ~ 0.6 , due to the onset of a large scale separation but the wave drag rise is not as regular as expected. Indeed an inspection of the flow field (not shown here) reveals that at low AoA , the main wave drag sources are located on the suction side of the lower wing tip whereas at high AoA , a large scale separation occurs near the tip of the lower wing, which prevents the development of the strong shock on the tip.

A nearly quadratic behaviour is observed for the induced drag which contributes for ~ 54 % of the total drag at the reference cruise conditions, i.e. at zero incidence. The aerodynamic efficiency L/D and the equivalent Oswald efficiency e are illustrated as a function of CL in Figure 16(c) and Figure 16(d), respectively. The maximum efficiency of ~ 23.8 is achieved close to the cruise design point, around $CL \sim 0.4$. As expected, for a boxwing architecture, the Oswald efficiency is always greater than 1, with $e=1.30$ at $CL=0.5$ and a maximum value of $e=1.315$ at $CL \sim 0.58$ which does not correspond to the maximum aerodynamic efficiency conditions. Then an abrupt decrease of e occurs at increased lift conditions. However, it should be noted that this incipient stall conditions fall outside the limits of the Prandtl's lifting line model and the related definition of e is rather pointless.



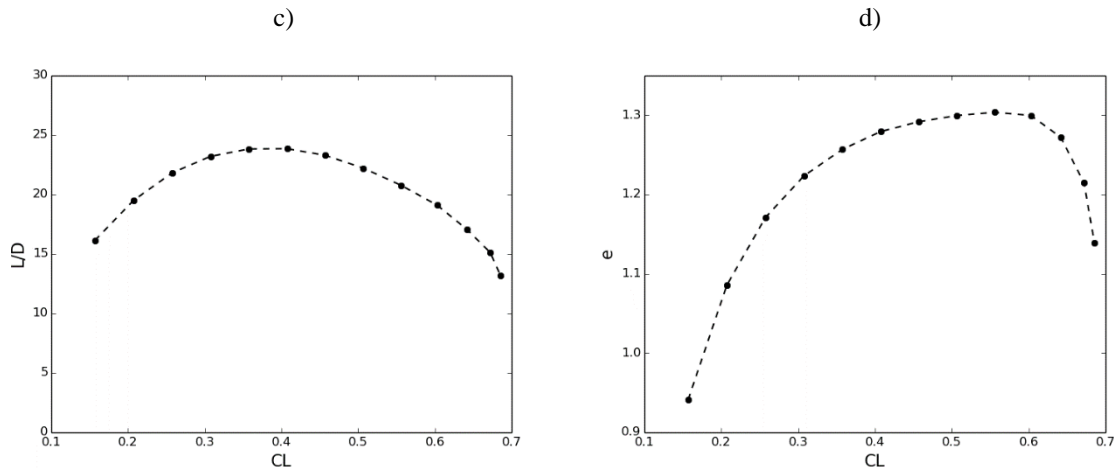


Figure 16. Cruise aerodynamic performance of the baseline boxwing configuration. (a) Lift curve. (b) Far-field drag polar curves. (d) Total efficiency as a function of C_L . (d) Equivalent Oswald efficiency as a function of C_L .

Table 2: Values of far-field drag coefficients for the baseline configuration and the configuration integrating the ONERA airfoils. Comparison of RANS and Euler predictions at reference cruise conditions, i.e. $M=0.79$, altitude of 11.0 km and $C_L=0.5$.

Boxwing Configuration	CFD Model	CD_{ff}	CD_f	CD_{vp}	CD_w	CD_i	L/D	e
Baseline	Euler	225.2	57.9 ^a	30.5 ^a	13.6	123.2	22.20	1.33
Baseline	RANS	224.1	57.9	30.5	9.5	126.2	22.31	1.30
ONERA airfoils	Euler	228.5	57.7 ^a	32.2 ^a	20.0	118.6	21.88	1.38
ONERA airfoils	RANS	225.0	57.7	32.2	14.9	120.2	22.22	1.36

^aFor the sake of comparison in terms of aerodynamic efficiency, RANS prediction are employed for both friction and viscous pressure drag contributions.

4.2 Euler-based optimisation of the twist distribution and CFD assessment

In order to improve the cruise aerodynamic performance of the boxwing lifting-system, aerodynamic optimizations have been performed using the CANOE suite developed at ONERA. This module is based on Euler CFD computations performed using the SU^2 code [35] and on the in-house ONERA far-field drag decomposition tool *ffd* presented above. In CANOE the surface meshes are automatically created from a boxwing geometrical model defined through OpenVSP [36], while the final unstructured volume meshes employed for the Euler computations are automatically generated by *Tetgen* [37]. To ensure an accurate and reliable evaluation of the total drag during the optimization process, a detailed parametric study with respect to mesh parameters has been achieved and coupled with the post-processing procedure using *ffd*.

The boxwing baseline geometry is parameterized by 8 control sections, as illustrated in Figure 17. For each of these sections the absolute twist angle referred to the airfoil leading edge is considered, with the twist distribution being assumed to linearly vary between two adjacent control sections. In addition to the baseline boxwing configuration, another boxwing configuration is also investigated. This additional configuration features the same wing planform of the baseline one but different airfoils at the control sections corresponding to transonic airfoil designed at ONERA in previous research projects (for instance the profiles of the ONERA NOVA configuration [38] for the front wing and typical backward swept wing profile for the rear wing). For both these baseline configurations, a comparison in terms of far-field drag components between the Euler-based modelling (through the CANOE suite) and RANS modelling (based on the *elsA* solver) is given in Table 2. The two approaches are rather consistent: as expected the shock drag is overestimated in Euler computations, thus impacting the optimisation process in a conservative way. On the contrary, the induced drag is only slightly underestimated, and thus the total drag quite accurately predicted w.r.t. higher fidelity computations.

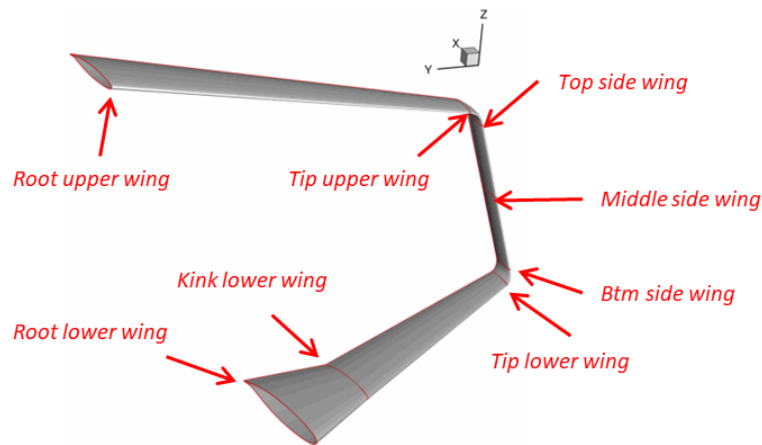


Figure 17. Control sections for the boxwing parameterisation and optimization.

For both the two considered boxwing configurations, multipoint optimizations have been carried out with the objective of minimizing the sum of the total drag for 3 lift conditions ($C_L=0.45, 0.50, 0.55$). The modified (*DOT-MMFD*) method of feasible directions of van der Plaats [39][40] available within the *Dakota* optimization library [41] is employed for such purpose. Such method is combined with a gradient descent technique, with the gradient being computed through a finite difference approach. For both the considered configurations, the computed optimisation histories are reported in Figure 18(a) by showing the evolution of the objective function and of the design variables. In Figure 18(b) the optimised twist distributions are also compared with the initial ones and the corresponding values for the considered control sections are reported in Table 3. In particular, on the front wing, both optimized configurations (baseline and baseline with ONERA airfoils) have almost the same distributions whereas on the rear wing, the optimal twist value at the root section is completely different. This can mainly be ascribed to the fact that for this section the shapes of the wing profiles are completely different, with a typical forward swept wing profile for the ONERA configuration.

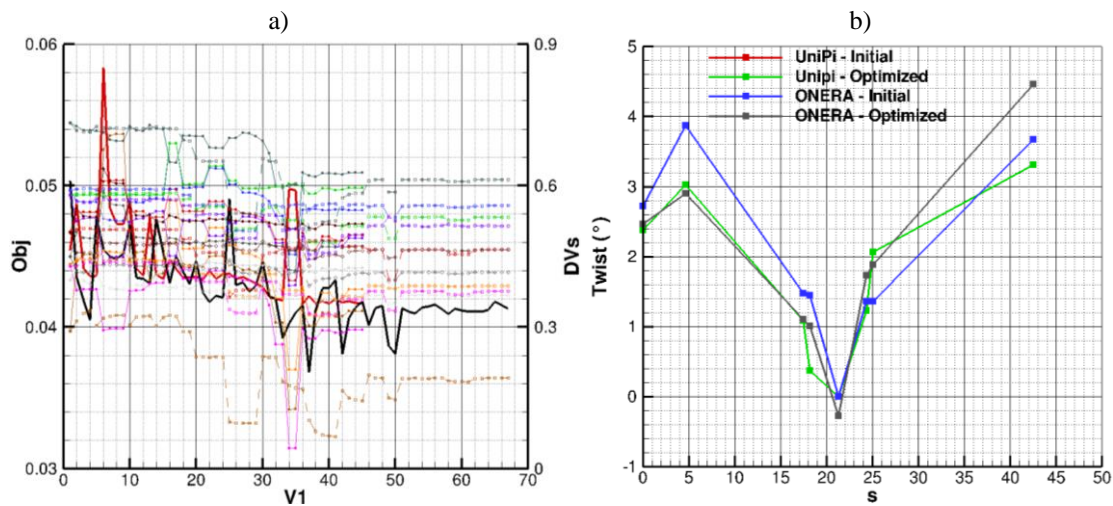
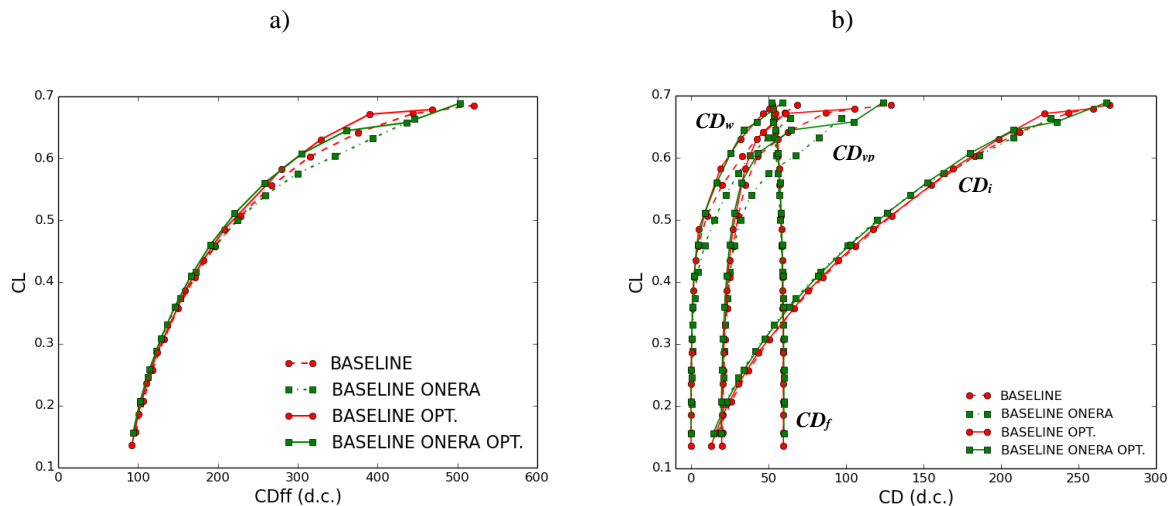


Figure 18: (a) Twist optimization results for both the baseline boxwing configuration (*Baseline*) and the new configuration integrating ONERA airfoils (*Baseline-ONERA*): optimization history of the objective function and of the non-dimensional twist variables. (b) Comparison of original and optimal twist distributions for both configurations. Note that $s=0$ corresponds to the root section of the front wing while $s=s_{max}$ corresponds to root section of the rear wing, s being a curvilinear abscissa defined along the axis of the boxwing. Values of s are given in m.

Table 3: Twist optimization results for both the baseline boxwing configuration (*Baseline*) and the new configuration integrating ONERA airfoils (*Baseline-ONERA*): detailed comparison of initial and optimised twist values at control sections. All values are reported in degrees.

Boxwing Configuration	Root lower wing	Kink lower wing	Tip lower wing	Btm side wing	Middle side wing	Top side wing	Tip upper wing	Root Upper wing
Baseline	2.721	3.869	1.468	1.441	0.04	1.361	1.368	3.668
Baseline optimised	2.383	3.017	1.037	0.358	-0.03	1.237	2.096	3.331
Baseline ONERA optimised	2.461	2.904	1.097	1.009	-0.28	1.731	1.881	4.464

The reduction of the objective function is relatively important and both the final optimized configurations feature very similar aerodynamic performances as reported in Table 4 where a detailed comparison between Euler and RANS far-field drag results is presented for $C_L=0.5$. For this considered value of the lift coefficient the optimised configuration integrating ONERA airfoils performs slightly better than the optimised baseline, both in terms of overall aerodynamic efficiency and Oswald efficiency, with a gain of nearly 10 d.c. for the total drag, mainly resulting from the consistent reduction of the wave drag, and of the viscous pressure drag. A more detail analysis is presented in Figure 19 by means of a RANS-based assessment of the optimised configurations w.r.t. the starting baselines for several incidences at cruise conditions. The far-field drag breakdown of Figure 19(b) clearly shows that for both configurations, the optimisation significantly reduces the wave drag rise at high incidences. For the ONERA design an important concomitant gain is also observed for the pressure viscous drag component, which can be ascribed to the different behaviour of the shock-induced separation at the lower wing tip. Concerning the induced drag, an opposite behaviour is observed for the two optimised designs, with the induced drag being slightly decreased/increased for the baseline/baseline-ONERA configurations, respectively. This is also confirmed by the Oswald efficiency in Figure 19(d). Notwithstanding, a higher Oswald efficiency is achieved when integrating the ONERA NOVA airfoils. For both configurations, the twist optimisation also allows to extend the nearly uniform Oswald efficiency range at higher values of C_L . A similar behaviour is also observed for the whole aerodynamic efficiency, illustrated in Figure 19(c) where, for both optimised designs, the efficiency is consistently improved in the C_L range tackled by the optimisation process up to $C_L=0.6-0.65$, without reducing the performance at lower C_L values. Finally, a consistent improvement of the overall efficiency is obtained by the optimised ONERA design with a maximal efficiency of ~ 24.6 compared to the value of ~ 23.8 for the optimised baseline.



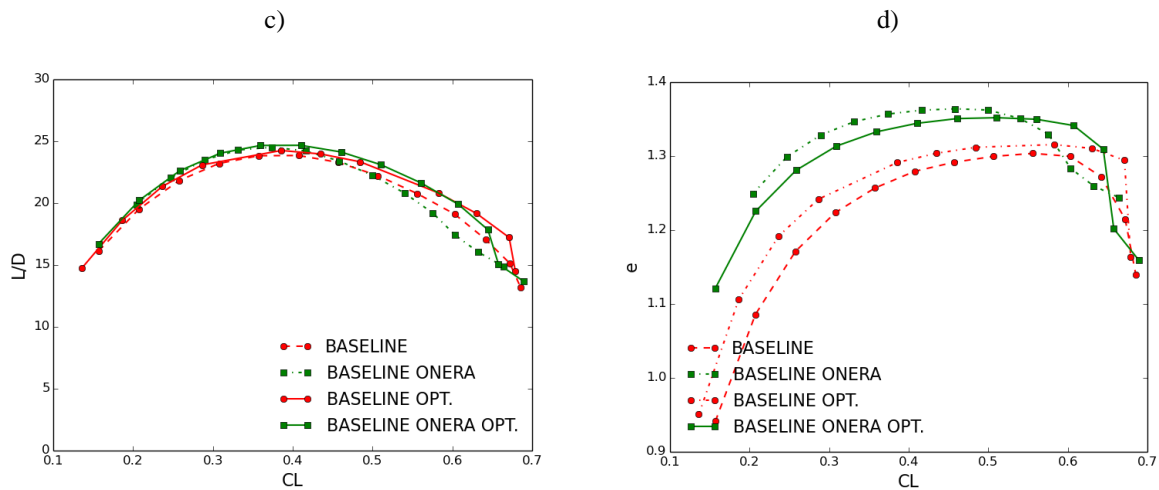


Figure 19: Comparison of cruise aerodynamic performance between initial and optimised designs. Results for both the baseline boxwing configuration (*Baseline*) and the new configuration integrating ONERA airfoils (*Baseline-ONERA*) are presented. (a) Polar. (b) Far-field drag polar curves. (d) Total efficiency as a function of C_L . (d) Equivalent Oswald efficiency as a function of C_L .

Table 4: Values of far-field drag coefficients for the baseline configuration and the configuration integrating the ONERA airfoils both using optimal twist values. Comparison of RANS and Euler predictions at reference cruise conditions, i.e. $M=0.79$, altitude of 11.0 km and $C_L=0.5$.

Opt. Boxwing Configuration	CFD Model	CD_{ff}	CD_f	CD_{vp}	CD_w	CD_i	L/D	e
Baseline	Euler	217.9	58.2 ^a	28.2 ^a	9.2	122.3	22.95	1.34
Baseline	RANS	219.0	58.2	28.2	7.2	125.4	22.83	1.31
ONERA airfoils	Euler	214.4	58.3 ^a	27.1 ^a	9.7	119.3	23.32	1.37
ONERA airfoils	RANS	214.5	58.3	27.1	7.8	121.3	23.31	1.35

^aFor the sake of comparison in terms of aerodynamic efficiency, RANS prediction are employed for both friction and viscous pressure drag contributions

5 Conclusion

Finding solutions for satisfying the growing air traffic demand in a sustainable way is a key subject for aviation research and industry. A possible way to face this problem is the development of disruptive configurations that are more efficient than the conventional aircraft. In this paper the aerodynamic analysis and design of an innovative configuration have been described; this configuration, called PrandtlPlane, is based on a box-wing architecture designed following the Best Wing System theory. The design process has been divided into three consecutive parts: in the first conceptual phase different concepts have been evaluated with low fidelity tools in order to identify the best solutions. Then, in the preliminary aerodynamic design, a reference configuration has been defined using both low and high fidelity tools. Finally, the reference configuration has been refined through an optimization procedure coupled with CFD simulations, in which the twist distribution has been considered as design variable. The results obtained from the whole aerodynamic design and analysis process highlights that the PrandtlPlane has high aerodynamic performances, in terms of lift-to-drag ratio, also in transonic conditions. Moreover, the PrandtlPlane configuration is capable to transport a larger payload with respect to the conventional competitors operating in the sector of continental routes, maintaining the same overall dimensions. These features can face the problems of growing air traffic demand, aircraft emissions per passenger and airport saturation. The aerodynamic performance of

the PrandtlPlane can be further improved; the next step of the aerodynamic development is represented by an aerodynamic optimization based on a larger design space defined by a larger number of design parameters.

Acknowledgments

The present paper presents part of the activities carried out within the research project PARSIFAL (“Prandtlplane ARchitecture for the Sustainable Improvement of Future AirpLanes”), which has been funded by the European Union under the Horizon 2020 Research and Innovation Program (Grant Agreement n.723149).

References

- [1] European Commission. Flightpath 2050: Europe’s Vision for Aviation. European Commission, Directorate General for Research and Innovation, Directorate General for Mobility and Transport, 2011
- [2] EREA. Study on the Air Transport System in 2050 from vision towards a planning for research and innovation. European Research Establishments in Aeronautics, 2012
- [3] ACARE, Strategic Research and Innovation Agenda (SRIA). Advisory Council for Aviation Research and Innovation in Europe, 2017
- [4] L. Prandtl, “Induced drag of multiplanes”, NACA Technical Note, no. 182, 1924.
- [5] Frediani, G. Montanari, “Best Wing System: An Exact Solution of the Prandtl’s Problem”, in “Variational Analysis And Aerospace Engineering”, Springer Dordrecht Heidelberg London New York, 2009, pp183-211.
- [6] Cipolla, V., Frediani, A., & Lonigro, E. (2016). Aerodynamic design of a light amphibious PrandtlPlane: wind tunnel tests and CFD validation. *Aerotecnica Missili & Spazio*, 94(2), 113-123. doi:http://dx.doi.org/10.19249/ams.v94i2.128
- [7] Oliviero, F., Zanetti, D., & Cipolla, V. (2016). Flight dynamics model for preliminary design of PrandtlPlane wing configuration with sizing of the control surfaces. *Aerotecnica Missili & Spazio*, 95(4), 201-210. doi:http://dx.doi.org/10.19249/ams.v95i4.289
- [8] Frediani, V. Cipolla, and F. Oliviero. "Design of a prototype of light amphibious PrandtlPlane", 56th AIAA/ASCE/AHS/ASC Structures, Structural Dynamics, and Materials Conference, AIAA SciTech Forum, (AIAA 2015-0700)
- [9] R. Cavallaro, L. Demasi, “Challenges, Ideas, and Innovations of Joined-Wing Configurations: A Concept from the Past, an Opportunity for the Future”, *Progress in Aerospace Sciences*, Volume 87, 2016, Pages 1-93, ISSN 0376-0421, http://dx.doi.org/10.1016/j.paerosci.2016.07.002.
- [10] Frediani, V. Cipolla, E. Rizzo, “The PrandtlPlane Configuration: Overview on Possible Applications to Civil Aviation” in Frediani, Buttazzo Eds. “Variational Analysis and Aerospace Engineering: Mathematical Challenges for Aerospace Design”, Volume 66 of the series Springer Optimization and Its Applications, pp 179-210, 2012.
- [11] Frediani, F. Oliviero, and E. Rizzo. "Design of an airfreight system based on an innovative PrandtlPlane aircraft", 56th AIAA/ASCE/AHS/ASC Structures, Structural Dynamics, and Materials Conference, AIAA SciTech Forum, (AIAA 2015-1186)
- [12] Beccasio N., Tesconi M., Frediani A. (2012) PrandtlPlane Propelled with Liquid Hydrogen: A Preliminary Study. In: Buttazzo G., Frediani A. (eds) *Variational Analysis and Aerospace Engineering: Mathematical Challenges for Aerospace Design*. Springer Optimization and Its Applications, vol 66. Springer, Boston, MA
- [13] Jemitola, P. O., & Fielding, J. P. (2012). Box wing aircraft conceptual design. In 28th Congress of the International Council of the Aeronautical Sciences (pp. 23-28).
- [14] PARSIFAL Project. European Commission, Horizon 2020 Research Programme. Call: H2020-MG-2016-2017, Topic MG-1.4-2016-2017 (Grant Agreement n. 723149)
- [15] PARSIFAL Project. 2018. Report on socio-economic scenarios and expectations. Project Deliverable D1.1. www.parsifalproject.eu
- [16] PARSIFAL Project. 2018. Requirements for the adoption of the PrandtlPlane as a mean of transport. Project Deliverable D2.1. www.parsifalproject.eu
- [17] Cipolla, V., A. Frediani, K. Abu Salem, M. Picchi Scardaoni, A. Nuti, V. Binante. 2018. Conceptual design of a box wing aircraft for the air transport of the future. AIAA Aviation Forum.
- [18] ICAO. 2009. Aerodromes: volume I – aerodrome design and operations. International standards and recommended practices, Annex 14.
- [19] European Commission. 2011. Europe’s Airports 2030: challenges ahead. Press release.
- [20] Raymer, D.P., 1999. Aircraft Design: a conceptual approach. AIAA Education Series.
- [21] Rizzo, E., 2007. Optimization methods applied to the preliminary design of innovative, non conventional aircraft configurations. PhD Thesis. Università di Pisa.
- [22] Drela, M., H. Youngren. 2010. AVL 3.30 User Primer. http://web.mit.edu/drela/Public/web/avl/

- [23] Frediani, A., V. Cipolla, K. Abu Salem, V. Binante, M. Picchi Scardaoni. 2019. Conceptual design of PrandtlPlane civil transport aircraft. Proceedings of the Institution of Mechanical Engineers, Part G: Journal of Aerospace Engineering.
- [24] Cappelli, L., G. Costa, V. Cipolla, A. Frediani, F. Oliviero, E. Rizzo. 2016. Aerodynamic optimization of a large PrandtlPlane configuration. *Aerotecnica, Missili & Spazio*.
- [25] Abu Salem, K., 2016. Studio sulla configurazione aerodinamica di velivoli civili di tipo PrandtlPlane di piccole e medie dimensioni. M.Sc. Thesis. Università di Pisa.
- [26] Cipolla, V., A. Frediani, K. Abu Salem., V. Binante, E. Rizzo, M. Maganzi. 2017. Preliminary transonic CFD analyses of a PrandtlPlane transport aircraft. *Transportation Research Procedia*.
- [27] Beltramo, M., D. Trapp, B. Kimoto, D. Marsh. 1977. Parametric study of transport aircraft systems cost and weight. Report NASA CR 151970.
- [28] Picchi Scardaoni, M., V. Binante, V. Cipolla. 2017. WAGNER: a new code for parametrical structural study of fuselages of civil transport aircraft. *Aerotecnica, Missili & Spazio*.
- [29] <http://elsa.onera.fr/Cassiopee/>
- [30] Spalart, P. R., and Allmaras, S. R.. 1992. "A One-Equation Model for Aerodynamic Flows", AIAA paper 92-0439, 30th AIAA Aerospace Sciences Meeting and Exhibit, Reno, NV, Jan. 6-9, 1992.
- [31] Spalart, P. R. 2000. "Strategies for Turbulence Modelling and Simulation", *International Journal of Heat and Fluid Flow*, 21(3): 252–263.
- [32] Jameson, A., Schmidt, W., Turkel, E. 1981. "Numerical solutions of the Euler equations by finite volume methods using Runge-Kutta time-stepping schemes". AIAA paper 1259.
- [33] van der Vooren J. and Destarac, D., 2004. "Drag/Thrust Analysis of Jet-propelled Transonic Transport Aircraft; Definition of Physical Drag Components," *Aerospace Science & Technology* 8:545-556.
- [34] Destarac D. 2003. "Far-field / Near-field Drag Balance and Applications of Drag Extraction in C.F.D." VKI Lecture Series, CFD Based Aircraft drag Prediction and Reduction, Hampton VA.
- [35] Economon T. D., Palacios F., Copeland S. R., Lukaczyk T. W., and Alonso J. J., 2016. "SU2: An open-source suite for multiphysics simulation and design", *AIAA Journal*, 54(3):828-846.
- [36] Chaput, A., Rizo-Patron, S., 2012. Vehicle Sketch Pad Structural Analysis Module Enhancements for Wing Design, 50th AIAA Aerospace Sciences Meeting, Nashville, TN, AIAA-2012-546.
- [37] Hang Si. 2015. TetGen, a Delaunay-Based Quality Tetrahedral Mesh Generator. *ACM Trans. on Mathematical Software*. 41 (2), 2015. <http://doi.acm.org/10.1145/2629697>.
- [38] Wiart L., Atinault O., Grenon G., Paluch B., and Hue D.. 2015. "Development of NOVA aircraft configurations for large engine integration studies". In 33rd AIAA Applied Aerodynamics Conference.
- [39] Van der Plaats G. N., 1984. "Numerical Optimization Techniques for Engineering Design with Applications", Mc Graw-Hill.
- [40] Van der Plaats G. N., 1995. "DOT user's manual", version 4.20.
- [41] Dakota: Design Analysis Kit for Optimization and Terascale Applications. Developed by SANDIA National